JOURNAL OF SOLID STATE CHEMISTRY 114, 499–505 (1995)

Magnetic Properties of Fresnoite-Type Vanadium Oxides: $A_2V_3O_8$ (A = K, Rb, NH_4)

Guo Liu and J. E. Greedan[1]

Institute for Materials Research, McMaster University, 1280 Main Street West, Hamilton, Ontario L8S 4M1, Canada

Received March 8, 1994; in revised form June 13, 1994; accepted June 16, 1994

Methods for synthesizing large amounts of polycrystalline $A_2V_3O_8$ (A = K, Rb, and NH_4) are introduced. Crystals of $Rb_2V_3O_8$ have been grown in a RbBr flux and the crystal structure has been confirmed by single crystal X-ray diffraction. Magnetic susceptibility data of these fresnoite-type vanadium oxides are presented. All three compounds exhibit short-range magnetic correlations below 10 K. The susceptibility data are analyzed based on a two-dimensional square-planar model. The interactions are antiferromagnetic and the magnitude of the exchange ($-J/k$) decreases in the order $K_2V_3O_8$, $Rb_2V_3O_8$, and $(NH_4)_2V_3O_8$.

INTRODUCTION

Fresnoite ($Ba_2TiSi_2O_8$) has a two-dimensional structure that consists of layers of corner-sharing Si_2O_7 groups and TiO_5 square pyramids with the large cation (Ba^{2+}) lying between the layers in the pentagonal prismatic channels (1–3). $Ba_2VSi_2O_8$ (4) and the $A_2V_3O_8$ family (A = K (5), Rb (6), Tl (7), and NH_4 (8, 9)) have been known to adopt this structure in which the magnetic V^{4+} ions form isolated VO_5 square pyramids. $Ba_2VSi_2O_8$ appears to be a simple paramagnet at temperatures down to 5 K (10). Except for $(NH_4)_2V_3O_8$ and $K_2V_3O_8$, which have been the subjects of recent ESR (EPR) studies and very limited low-temperature magnetic susceptibility measurements (8, 11), little was known about the magnetic properties of the $A_2V_3O_8$ family. The preliminary work suggested a possible antiferromagnetic interaction with estimated Curie temperatures $\theta = -1.3$ K for $(NH_4)_2V_3O_8$ (8) and -3.7 K for $K_2V_3O_8$ (11).

The fresnoite-type vanadium oxides are interesting because of the pseudo-cubic arrangement of the magnetic ions. The crystal structure of a fresnoite-type $A_2V_3O_8$ is shown in Fig. 1a and projected along the c-axis in Fig. 1b. To distinguish the magnetic V^{4+} ions from the nonmagnetic V^{5+} ions only the square pyramides of V^{4+} are shaded in Fig. 1. Each V^{4+} ion has six nearest neighboring magnetic ions. It will be shown later that the ratio of the nearest $V^{4+} \cdots V^{4+}$ distance within a layer to that between the layers ranges from 1.128 for $(NH_4)_2V_3O_8$ to 1.198 for $K_2V_3O_8$. Therefore the magnetic sublattice can be roughly considered a simple cube. This family is thus similar to Ba_3CrO_5 which has been shown to undergo a 3D magnetic phase transition at $T_c \approx 8$ K (12). In this work new methods to synthesize large quantities of powder specimens of $A_2V_3O_8$ (A = K, Rb, NH_4) are described and magnetic susceptibility data are presented.

EXPERIMENTAL

Materials Preparation

V_2O_3 was prepared by reducing V_2O_5 (Cerac, 99.9%) under H_2 at 900°C. KVO_3 was prepared according to the method described in reference (13). A stoichiometric mixture of predried K_2CO_3 (BDH Chemicals, assured) and V_2O_5 was heated in a Pt crucible at 365°C overnight, at 500°C for 1 hr, then at 1000°C for 1 hr, and finally, furnace cooled. $RbVO_3$ was prepared by heating a stoichiometric mixture of Rb_2CO_3 (Johnson Matthey Catalog Co., 99.8% on metal basis) and V_2O_5 at 600°C for 24 hr. Moisture-sensitive materials K_2CO_3, Rb_2CO_3, KVO_3, and $RbVO_3$ were handled in an argon-filled glove box when necessary.

$K_2V_3O_8$. A mixture of KVO_3, V_2O_3, and V_2O_5, which were weighed in the glove box in an 8 : 1 : 1 molar ratio, was ground intimately, pelleted quickly in air, and sealed in Pyrex under a 10^{-4} Torr pressure. The mixture was heated at 550°C for 24 hr and cooled slowly. A deep violet product of $K_2V_3O_8$ was obtained.

$Rb_2V_3O_8$. It was prepared in a similar way to $K_2V_3O_8$ using an 8 : 1 : 1 mixture of $RbVO_3$, V_2O_3, and V_2O_5. This phase was also obtained as a mixture with about 80% $Rb_2V_4O_9$ when a 2 : 1 mixture of $RbVO_3$ and V_2O_3 was heated at 550°C overnight in a sealed tube. Pure $Rb_2V_3O_8$ is also deep violet.

$(NH_4)_2V_3O_8$. One to two grams of a 9 : 1 mixture of NH_4VO_3 (purified Fisher Scientific) and V_2O_3 was ground intimately, pelleted, and sealed in Pyrex (11.5 mm o.d.

[1] To whom correspondence should be addressed.

0022-4596/95 $6.00

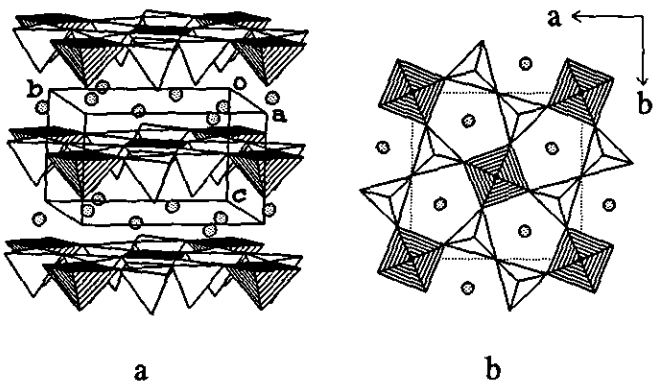

FIG. 1. (a) The structure of fresnoite type $A_2V_3O_8$ (A = K, Rb, Tl, and NH_4) and (b) projection down the c-axis. The shaded polyhedra are $V(IV)O_5$ square pyramids and the unshaded are $V(V)O_4$ tetrahedra. Shaded circles are Rb atoms.

and 1 mm thickness) under a 10^{-4} Torr pressure. The sample was heated slowly at 2°C/min to 250°C and soaked for 6–12 hr, and then furnace-cooled. Once cooled, the tube was immediately and cautiously cut open with a diamond saw. Deep violet specimens were obtained. Condensed moisture was observed on the walls of the tube and the presence of ammonia gas was evident.

Crystal growth of $Rb_2V_3O_8$. About 2-g mixtures containing 5 to 10% $Rb_2V_3O_8$ by weight, or 15% of the 20% $Rb_2V_3O_8$ + 80% $Rb_2V_4O_9$ mixture with RbBr (99.9%, Cerac. M.P. 693°C), were evacuated and sealed in quartz under a 10^{-4} Torr pressure, heated to 750°C slowly (~5°C/m), and cooled at a rate of 6°C/hr to 500°C, and finally at 30°C/hr to room temperature. The flux was removed by washing with distilled water. Plate-like crystals of $Rb_2V_3O_8$ were obtained.

X-ray Diffraction and Magnetic Mesurements

Preliminary examinations were performed using a Guinier-Hägg camera with Cu$K\alpha_1$ radiation and a Si standard. The Guinier data were read with a computer-controlled, automated LS-20 type line scanner (KEJ INSTRUMENTS, Täby, Sweden). Magnetic susceptibility data were obtained using a Quantum Design SQUID magnetometer in the temperature range 3 to 300 K for $(NH_4)_2V_3O_8$ and 5–300 K for other samples. The procedures for single crystal X-ray diffraction have been described elsewhere in detail (10).

RESULTS AND DISCUSSION

All the polycrystalline specimens of $A_2V_3O_8$ (A = K, Rb, and NH_4) were phase-pure and well-crystallized as shown by their powder diffraction patterns (Tables 1–3). Derived cell parameters are compiled in Table 4 together with some literature values. They agree well in general.

Previously reported methods for the synthesis of $(NH_4)_2V_3O_8$ mainly involve chemical or electrochemical reduction of V_2O_5 in ammonium salt solutions (14, 15). Single crystals of $(NH_4)_2V_3O_8$ have been grown by hydrothermal methods (8, 9). None of the methods is simple and suitable for preparing relatively large amounts of pure polycrystalline $(NH_4)_2V_3O_8$. Solid state methods were generally considered not applicable because of the low thermal stability of ammonia vanadates. A rather early reference suggested that $(NH_4)_2V_3O_8$ could be prepared by reacting a stoichiometric mixture of $2NH_4VO_3$ and VO_2 at 250°C in sealed tubes (15). Our repeated experiments suggested that it was not possible to make a single phase $(NH_4)_2V_3O_8$ by that method. Instead the product contained up to 40% $NH_4V_4O_9$. Excess NH_3 gas was evident and condensed water was observed when the tube was opened. Apparently the decomposition of NH_4VO_3 had occurred.

NH_4VO_3 starts to decompose at ~200°C under normal pressure according to

$$2NH_4VO_3 \xrightarrow{\sim 200°C} V_2O_5\,(s) + 2NH_3\,(g) + H_2O\,(g). \quad [1]$$

To take advantage of the formation of V_2O_5 in this decomposition reaction, V_2O_3 was used to convert it into VO_2 by an anti-disproportionation reaction. Thus a new solid

TABLE 1
Powder X-ray Diffraction Pattern of $K_2V_3O_8$

h	k	l	d(cal)	d(obs)	I(obs)
0	0	1	5.247	5.242	39
1	1	1	4.029	4.027	4
2	1	0	3.9768	3.9764	15
2	0	1	3.3921	3.3915	26
2	1	1	3.1693	3.1688	100
3	1	0	2.8121	2.8118	37
0	0	2	2.6234	2.6226	15
3	1	1	2.4785	2.4774	9
3	2	0	2.4663	2.4661	3
4	0	0	2.2231	2.2232	7
4	1	0	2.1567	2.1566	6
3	3	0	2.0960	2.0956	4
4	1	1	1.9948	1.9937	7
4	2	0	1.9884	1.9887	14
5	1	1	1.6549	1.6556	12
2	1	3	1.6010	1.6009	12
5	2	1	1.5751	1.5752	15
4	4	0	1.5720	1.5717	7
3	0	3	1.5063	1.5061	5
3	1	3	1.4851	1.4847	5

TABLE 2
Powder X-ray Diffraction Pattern of $Rb_2V_3O_8$

h	k	l	d(cal)	d(obs)	I(obs)
1	1	0	6.308	6.298	2
0	0	1	5.541	5.535	3
1	1	1	4.163	4.160	3
2	0	1	3.4745	3.4734	24
2	1	1	3.2376	3.2370	100
2	2	0	3.1539	3.1526	10
3	1	0	2.8209	2.8205	40
0	0	2	2.7706	2.7705	12
3	1	1	2.5139	2.5149	3
3	2	0	2.4741	2.4736	2
2	0	2	2.3535	2.3540	3
2	1	2	2.2756	2.2758	6
3	2	1	2.2591	2.2586	3
4	0	0	2.2301	2.2301	6
4	1	0	2.1635	2.1634	16
3	3	0	2.1026	2.1023	11
4	1	1	2.0154	2.0155	10
4	2	0	1.9947	1.9945	12
3	1	2	1.9766	1.9765	12
3	3	1	1.9658	1.9658	7
0	0	3	1.8470	1.8468	2
5	1	0	1.7495	1.7491	2
4	0	2	1.7372	1.7370	2
2	0	3	1.7065	1.7057	6
4	1	2	1.7052	1.6759	16
2	1	3	1.6761	1.6683	8
5	1	1	1.6683	1.6187	2
4	2	2	1.6188	1.5871	17
5	2	1	1.5871	1.5769	6
4	4	0	1.5769	1.5298	3
5	3	0	1.5299	1.5170	3
4	4	1	1.5167	1.4866	6
6	0	0	1.4868	1.4662	3
6	1	0	1.4665	1.4049	4
4	1	3	1.4048	1.3881	3
3	3	3	1.3877	1.3668	6
6	2	1	1.3669	1.3511	3
5	4	1	1.3511	1.3100	5
6	0	2	1.3100	1.2434	4
3	1	4	1.2434	1.2329	5
5	2	3	1.2332	1.2253	2
7	2	0	1.2253	1.1990	2
4	4	3	1.1993	1.1715	3
7	3	0	1.1713		

TABLE 3
Powder X-ray Diffraction Pattern of $(NH_4)_2V_3O_8$

h	k	l	d(cal)	d(obs)	I(obs)
0	0	1	5.577	5.571	100
2	0	0	4.450	4.453	6
2	1	0	3.980	3.979	58
2	0	1	3.4782	3.4780	15
2	1	1	3.2396	3.2396	92
3	1	0	2.8141	2.8144	33
0	0	2	2.7887	2.7893	19
3	1	1	2.5124	2.5127	20
3	2	0	2.4681	2.4693	3
2	1	2	2.2838	2.2835	7
3	2	1	2.2570	2.2572	5
4	2	0	1.9899	1.9897	14
3	1	2	1.9808	1.9816	12
4	2	1	1.8742	1.8747	8
5	1	0	1.7452	1.7451	6
5	1	1	1.6656	1.6655	8
5	2	1	1.5844	1.5848	9
4	4	0	1.5731	1.5732	10
3	1	3	1.5512	1.5511	7
4	4	1	1.5141	1.5139	8
3	2	3	1.4850	1.4847	6
6	1	0	1.4630	1.4631	4
6	1	1	1.4151	1.4155	3
4	4	2	1.3702	1.3704	5
6	1	2	1.2955	1.2953	6
5	1	3	1.2724	1.2722	4
5	2	3	1.2351	1.2349	6
4	4	3	1.2009	1.2012	5

state method for the preparation of $(NH_4)_2V_3O_8$ was proposed according to

$$10NH_4VO_3 + V_2O_3 \xrightarrow[\text{sealed tube}]{250^\circ C} 4(NH_4)_2V_3O_8\,(s) + 2NH_3\,(g) + H_2O\,(g). \quad [2]$$

In practice, when a 10:1 mixture was used, trace amounts of tiny white particles (presumably NH_4VO_3) could be seen sometimes in the bulk pellets, though not detectable by X-ray diffraction. Thus the best molar ratio is between 9:1 and 9.5:1. The product was relatively well crystallized and pure as determined by X-ray diffraction. Its powder X-ray diffraction pattern (Table 3) matched in principle that reported by Bernard and coworkers (16). Derived cell parameters are slightly larger than theirs, but are comparable with those of single crystals obtained by hydrothermal methods.

TABLE 4
Cell Parameters and Axial Ratios for $A_2V_3O_8$ (A = K, Rb, and NH_4)

Compound	a(Å)	c(Å)	V(Å³)	$a' = a/\sqrt{2}$	a'/c	Reference
$K_2V_3O_8$	8.8925(6)	5.2468(6)	414.9(1)	6.2879	1.198	This work[a]
	8.870(6)	5.215(5)	410.30(5)	6.272	1.203	(5)[b]
$Rb_2V_3O_8$	8.9205(3)	5.5411(5)	440.94(8)	6.3077	1.138	This work[a]
	8.9229(7)	5.5449(9)	441.5(1)	6.3094	1.138	(6)[b]
$(NH_4)_2V_3O_8$	8.8990(7)	5.5773(8)	441.7(1)	6.2925	1.128	This work[a]
	8.891(4)	5.582(2)	441.3(3)	6.287	1.126	(8)[b]
	8.885(2)	5.5640(5)	439.2(1)	6.283	1.129	(9)[b]
$Cs_2V_3O_8$	8.940(3)	5.964(6)	476.7(8)	6.322	1.060	(17)

[a] Values from Guinier X-ray diffraction data. See text for details.
[b] Data obtained from single crystals.

TABLE 5
Summary of Crystallographic Data for $Rb_2V_3O_8$

Color, habit	brown/pink, plate
Crystal size (mm^3)	0.083 × 0.063 × 0.025
Crystal system	Tetragonal
Space group	*P4bm*
Unit cell dimensions	a = 8.9140(10) Å, c = 5.536(2) Å
Volume	439.9(3) Å^3
Z	2
Diffractometer used	Siemens P3
Scan type and range	ω, 0.06°
Scan speed (°/min)	Variable; 2.00 to 29.30
Radiation	Ag$K\alpha$ (λ = 0.56086 Å)
Monochromator	Graphite
Absorption correction	Semi-empirical
Index ranges	$0 \le h \le 13$, $0 \le k \le 13$, $-8 \le l \le 8$
Reflections collected	1593
Independent reflections	863 (R_{int} = 3.81%)
Observed reflections	380 ($F \ge 4.0\sigma(F)$)
Refinement method	Full-matrix least-squares
Quantity minimized	$\Sigma w(F_o - F_c)^2$
Weighing scheme	$1/w = \sigma^2(F)$
No. of parameters refined	37
Final R indices (obs. data)	R = 3.73%, R_w = 2.57%
Goodness-of-fit	0.75
Data-to-parameter ratio	10.3 : 1

A recent study reported the synthesis of the previously unknown $Cs_2V_3O_8$ by an electrochemical deposition method (17). It was said to be isostructural with fresnoite as well. A preliminary experiment using the method described for the synthesis of $K_2V_3O_8$ and $Rb_2V_3O_8$ produced only the $Cs_2V_4O_9$ phase.

Crystal Structures

$K_2V_3O_8$ and $(NH_4)_2V_3O_8$ have been shown by single crystal X-ray diffraction to have the fresnoite structure (5, 8, 9). Just when our single crystal work on $Rb_2V_3O_8$ was completed, another report on its crystal structure determination appeared (6). Our results are essentially the same as those reported, confirming that crystals grown in a RbBr flux are indeed $Rb_2V_3O_8$. The crystallographic data are summarized in Table 5 and atomic parameters in Table 6. The metals (Rb and V) were located by direct methods and oxygens by difference Fourier. Important bond lengths for $K_2V_3O_8$, $Rb_2V_3O_8$, and $(NH_4)_2V_3O_8$ are compared in Table 7. The V(2)O_4 tetrahedra in the three compounds are nearly of the same size. The V(1)O_5 square pyramid in $K_2V_3O_8$, however, appears to be slightly smaller than those in $Rb_2V_3O_8$ and $(NH_4)_2V_3O_8$.

All the vanadium oxides in this family have an ordered fresnoite structure; 2/3 of the vanadium ions are V^{5+} and form the isolated VO_4^{3-} tetrahedra and 1/3 of them are V^{4+} and form the VO_5^{6-} square pyramids as shown in Fig. 1.

Magnetic Properties

Temperature dependencies of the magnetic susceptibility and inverse susceptibility of $K_2V_3O_8$, $Rb_2V_3O_8$, and $(NH_4)_2V_3O_8$ are shown in Figs. 2–4, respectively. All three samples have a relatively broad susceptibility maximum below ~15K, indicating short-range magnetic correlations.

The high temperature data fit well to the Curie–Weiss law plus a temperature-independent term, $\chi_m = C/(T - \theta) + \chi_{TIP}$. The fitted parameters are compiled in Table 8. Consistent with the trend in the susceptibility maximum temperature, the magnitude of θ decreases in the order $K_2V_3O_8$, $Rb_2V_3O_8$, and $(NH_4)_2V_3O_8$. The observed Curie constants are only slightly lower than the spin-only value of 0.375 emu-K/mole for an S = 1/2 system, confirming the existence of V(IV) as suggested by the crystal structure.

It is worth noting that the Curie temperatures (θ) for $K_2V_3O_8$ and $(NH_4)_2V_3O_8$ are substantially more negative than those estimated from the EPR data (8, 11). The previously reported susceptibility data for $(NH_4)_2V_3O_8$ are only available for the temperature range of 1.5 to 4.1

TABLE 6
Atomic Coordinates and Temperature Factors[a] (Å^2 × 10^3) for $Rb_2V_3O_8$

	x	y	z[b]	U(eq)	U_{11}	U_{22}	U_{33}	U_{12}	U_{13}	U_{23}
Rb	0.6698(1)	0.1698(1)	0.65	29(1)	32(1)	$= U_{11}$	23(1)	−17(1)	0(1)	$= U_{13}$
V(1)	0	0	0.1196(12)	16(1)	13(1)	$= U_{11}$	21(3)	0	0	0
V(2)	0.3670(2)	0.1330(2)	0.1235(8)	14(1)	11(1)	$= U_{11}$	21(2)	0(1)	1(1)	$= U_{13}$
O(1)	0	0	0.4020(29)	23(4)	20(6)	$= U_{11}$	28(8)	0	0	0
O(2)	0.1939(7)	0.0842(7)	0.0133(11)	20(2)	14(4)	13(4)	33(3)	−2(3)	−1(3)	−5(3)
O(3)	0.5	0	0.0035(22)	17(3)	14(5)	$= U_{11}$	22(8)	O(7)	0	0
O(4)	0.3701(8)	0.1299(8)	0.4135(16)	21(2)	17(4)	$= U_{11}$	28(5)	2(5)	3(3)	$= U_{13}$

[a] Equivalent isotropic U defined as ⅓ the trace of the orthogonalized U_{ij} tensor. The anisotropic displacement exponent takes the form $-2\pi^2(h^2a^{*2}U_{11} + \ldots 2hka^*b^*U_{12})$.

[b] The z value for Rb was fixed to the arbitrary value in order to compare with reported results (6).

TABLE 7
Important Bond Lengths (Å) and Angles (°) for $A_2V_3O_8$ (A = K, Rb, NH_4)[a]

Compound:		$K_2V_3O_8$	$Rb_2V_3O_8$		$(NH_4)_2V_3O_8$	
Reference:		(5)	This work	(6)	(8)	(9)
A–O(1)	2×	3.512(6)	3.583(6)	3.576(2)		
A–O(2)	2×	2.875(6)	2.983(6)	2.996(3)		
A–O(2)′	2×	3.191(6)	3.263(6)	3.284(3)		
A–O(3)	1×	2.794(5)	2.901(8)	2.911(3)		
A–O(4)	2×	2.907(11)	2.996(7)	2.984(3)		
A–O(4)′	1×	2.769(11)	2.844(10)	2.911(3)		
Mean		3.053(7)	3.140(7)	3.150(3)		
V(1)–O(1)	1×	1.582(5)	1.564(17)	1.594(6)	1.650(8)	1.576(5)
V(1)–O(2)	4×	1.945(5)	1.974(7)	1.970(2)	1.962(3)	1.972(2)
Mean		1.872(5)	1.892(9)	1.895(3)	1.900(4)	1.893(3)
V(2)–O(2)	2×	1.699(5)	1.715(7)	1.711(3)	1.709(3)	1.721(2)
V(2)–O(3)	1×	1.794(4)	1.804(5)	1.806(5)	1.793(2)	1.803(2)
V(2)–O(4)	1×	1.628(11)	1.606(10)	1.631(4)	1.660(5)	1.618(3)
Mean		1.705(6)	1.710(7)	1.715(4)	1.718(3)	1.716(2)

[a] Atom labels are rearranged according to this work.

K and are apparently different from the observed data presented here.

To understand the origin and type of the magnetic exchange interactions in these systems, the three basic short-range models: 1D (infinite linear chain), dimer, and the 2D (square-planar) were tested to fit the susceptibility data. The dimer model is apparently unlikely based on the crystal structure, but was tested for completeness. These oxides are S = 1/2 systems. There is no zero-field splitting. From previous EPR results, at least in the $K_2V_3O_8$ and $(NH_4)_2V_3O_8$ systems, the g-factors are only slightly anisotropic (8, 11). Thus the Heisenberg model was used for the data fitting. The best fit was obtained with the 2D model. The formula used in the 2D fitting can be written as

$$\chi_m = \frac{N\mu_B^2 g^2}{2|J|}\left[3x + \sum_{n=1}^{6}\frac{C_n}{x^{n-1}}\right]^{-1} + \frac{C}{T-\theta} + \chi_{TIP}, \quad [3]$$

where $x = kT/2|J|S(S+1)$, J is the exchange parameter, g the powder-averaged g-factor, μ_B the Bohr magneton ($N\mu_B^2/k$ = 0.3751), S the spin quantum number, and C_n are constants which have been tabulated by Lines (18). The first term is the high-temperature series expansion for a 2D Heisenberg system according to Lines (18), the second Curie–Weiss term corrects for contributions from

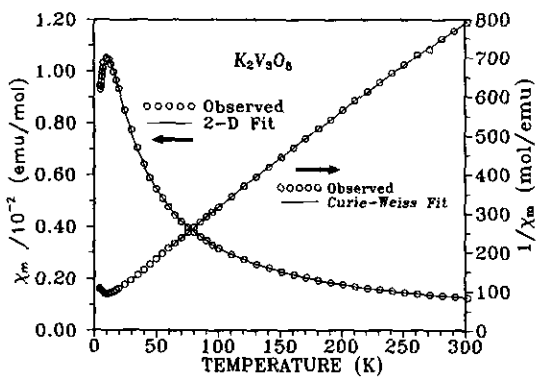

FIG. 2. Thermal variations of the magnetic susceptibility and inverse susceptibility data of $K_2V_3O_8$.

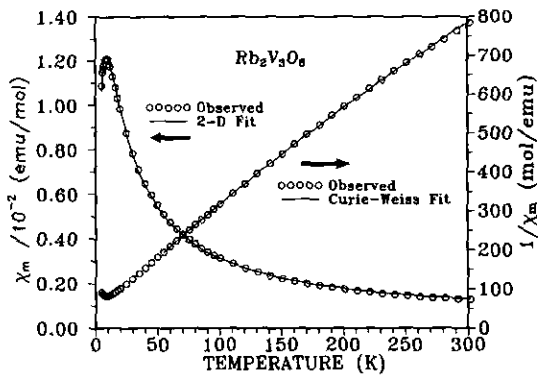

FIG. 3. Thermal variations of the magnetic susceptibility and inverse susceptibility data of $Rb_2V_3O_8$.

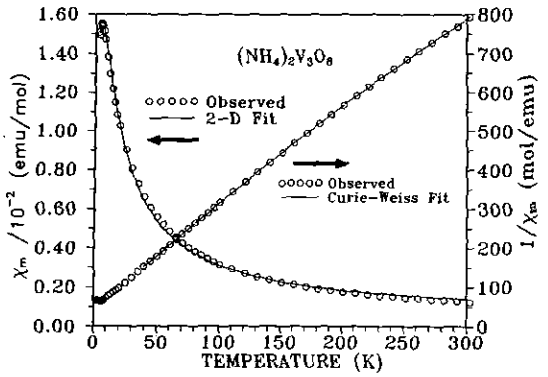

FIG. 4. Thermal variations of the magnetic susceptibility and inverse susceptibility data of $(NH_4)_2V_3O_8$.

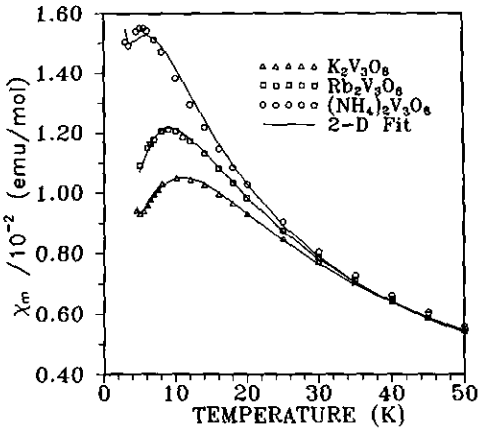

FIG. 5. Comparison of observed and fitted susceptibility data in the low temperature range for $A_2V_3O_8$ (A = K, Rb, NH_4)

trace amounts of impurities that were sometimes observed at very low temperatures, and χ_{TIP} is the temperature-independent paramagnetic susceptibility. The 1D (19) and dimer (20) models have been described previously. The fitting results are summarized in Table 8. The low temperature range of the observed and calculated susceptibility data for the three compounds is shown in Fig. 5, and the whole temperature range is shown individually in Figs. 2–4. The calculated data for the 1D and dimer models are omitted for clarity.

Judging from the R-factors, it is clear that the dimer model was not appropriate at all. Though the 1D model could fit the data reasonably well, it is not as good as the 2D model. The latter is consistent with the two-dimensional structure of these fresnoite type vanadium oxides. Even though their magnetic ion sublattice is a close approximation to a simple cubic lattice, as can be seen from the axial ratios (a'/c) in Table 4, magnetic exchange interactions within the layers perpendicular to the c-axis are expected to be much stronger than those between the layers. Within the ab plane, magnetic super-exchange would most likely occur through the $V(1)^{4+}$–O–$V(2)^{5+}$–O′–$V(1)^{4+}$ or $V(1)^{4+}$ or $(V1)^{4+}$–O–O′–$V(1)^{4+}$ (face diagonal in Fig. 6a) pathway. It is not possible to draw separate "chains" because the two diagonals are equivalent due to the tetragonal symmetry. Such a mechanism is thus two-dimensional. One-dimensional exchange coupling would only be possible between the V^{4+} ions of adjacent planes as suggested by Theobald and co-workers (8), that is, through a one-oxygen (V–O · · · V′) pathway involving the axial oxygens indicated in Fig. 6b using the dotted lines. Because that pathway would involve the extremely long O · · · V′ distance (~3.665 Å for $K_2V_3O_8$), the interaction would be expected to be extremely weak. Thus it can be concluded that the short-range order is antiferromagnetic and two-dimensional, at least for

TABLE 8
Summary of Magnetic Parameters for $A_2V_3O_8$ (A = K, Rb and NH_4)

Compound model	C (emu-K/mol)	θ (K)	$\chi_{TIP} \times 10^4$ (emu/mol)	J/k (K)	g	$\chi_{TIP} \times 10^4$ (emu/mol)	R^a (%)
$K_2V_3O_8$							
Curie-Weiss	0.346	−15.7	1.71				0.172
2D				−6.29	1.89	1.82	0.453
1D				−8.96	1.82	3.37	1.15
Dimer				−7.39	1.43	12.4	11.1
$Rb_2V_3O_8$							
Curie-Weiss	0.330	−12.4	2.19				0.175
2D				−4.96	1.83	3.03	0.829
1D				−7.48	1.78	4.03	1.35
Dimer				−7.19	1.51	10.1	7.08
$(NH_4)_2V_3O_8$							
Curie-Weiss	0.332	−11.7	2.02				0.219
2D				−3.85	1.73	4.74	1.79
1D				−5.00	1.64	7.25	3.83
Dimer				−4.88	1.40	13.2	9.26

[a] The agreement factor R is defined as R (%) = $100\sqrt{\Sigma(\chi_{obs} - \chi_{cal})^2/\Sigma\chi^2_{obs}}$.

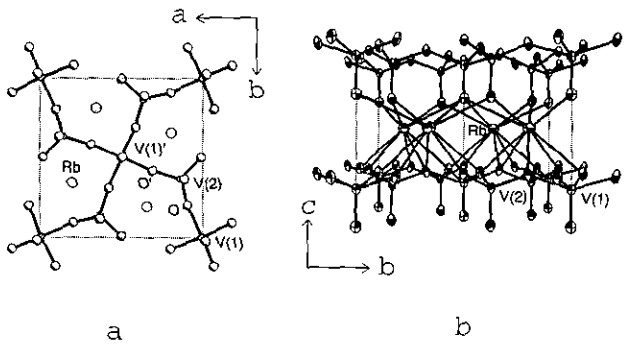

FIG. 6. Possible pathways for magnetic superexchange interactions in $A_2V_3O_8$ (A = K, Rb, NH_4). (a) Within a layer perpendicular to the c-axis; (b) between the layers.

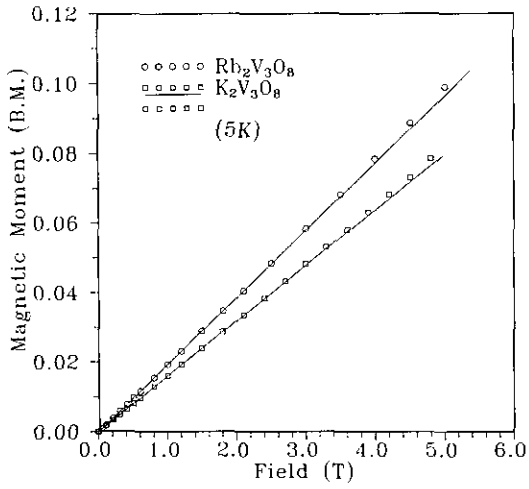

FIG. 7. Magnetization curves for $K_2V_3O_8$ and $Rb_2V_3O_8$ at 5 K showing a possible spin-flop transition.

$K_2V_3O_8$ and $Rb_2V_3O_8$. The fitting for $(NH_4)_2V_3O_8$ was not very satisfactory, especially in the low temperature range. Its magnetic behavior may have some 3D character. However, there is not enough evidence at this point to conclude that the susceptibility maximum at ~3.5K for $(NH_4)_2V_3O_8$ is due to the onset of long-range magnetic order.

The refined g-factor for $K_2V_3O_8$, 1.89, is rather close to the EPR value of ~1.94 (11), while the refined value for $(NH_4)_2V_3O_8$ (1.73) is apparently smaller than the EPR value of ~1.94 (11). The correlation of the exchange parameter $|J|/k$ with the a-axis and the V–O bond lengths is clear for $K_2V_3O_8$ and $Rb_2V_3O_8$, but not quite so for $(NH_4)_2V_3O_8$. The a-axis for $(NH_4)_2V_3O_8$ is shorter than that for $Rb_2V_3O_8$. It is not clear why $|J|/k$ is smaller for $(NH_4)_2V_3O_8$ than for $Rb_2V_3O_8$.

The magnetization curves for $K_2V_3O_8$ and $Rb_2V_3O_8$ at 5 K (Fig. 7) appear to show positive deviations from straight lines at higher magnetic fields, suggesting a spin-flop transition although the effect is not dramatic. Thus these materials may eventually undergo long-range order like Ba_3CrO_5 (12) but at a lower temperature. The difference in the magnetic behavior between the $A_2V_3O_8$ family and Ba_3CrO_5 is clear. Short-range correlations are important below ~15 K for the former, while they appear to be absent above T_c in the latter.

ACKNOWLEDGMENTS

The financial support of the Natural Science and Engineering Research Council of Canada and the Ontario Centre for Materials Research are acknowledged gratefully. We thank Dr. J. Britten for collecting the single crystal X-ray diffraction data and Professor C. V. Stager for use of the magnetometer.

REFERENCES

1. R. Masse, J.-C. Grenier, and A. Durif, *Bull. Soc. Fr. Mineral. Cristallogr.* **XC,** 20 (1967).
2. P. B. Moore and J. Louisnathan, *Science* **156,** 1361 (1967).
3. P. B. Moore and S. J. Louisnathan, *Z. Kristallogr.* **130,** 438 (1969).
4. A. Feltz, S. Schmalfuss, H. Langbein, and M. Tietz, *Z. Anorg. Allg. Chem.* **417,** 125 (1975).
5. J. Galy and A. Carpy, *Acta Crystallogr. Sect. B* **31,** 1794 (1975).
6. M.-L. Ha-Eierdanz and Ulrich Müller, *Z. Anorg. Allg. Chem.* **613,** 63 (1992).
7. J. Tudo, G. Laplace, and B. Jolibois, *C. R. Acad. Sci. Paris* Ser. **C,** 307 (1971).
8. F. R. Theobald, J.-G. Theobald, J. C. Vedrine, R. Clad, and J. Renard, *J. Phys. Chem. Solids* **45,** 581 (1984).
9. K.-J. Range, R. Zintl, and A. M. Heyns, *Z. Naturforsch. B.* **43,** 309 (1988).
10. Guo Liu and J. E. Greedan, *J. Solid State Chem.* **108,** 267 (1994).
11. M. Pouchard, F. Theobald, J. G. Theobald, R. Clad, and J. Renard, *Bull. Soc. Chim. Belg.* **97,** 241 (1988).
12. Guo Liu, J. E. Greedan, and Wenhe Gong, *J. Solid State Chem.* **105,** 78 (1993).
13. R. S. Feigelson, G. W. Martin, and B. C. Johnson, *J. Cryst. Growth* **13/14,** 686 (1972).
14. P. G. Dickens, S. J. Hibble, and R. H. Jarman, *J. Electrochem. Soc.* **130,** 1787 (1983).
15. J. Tudo, G. Laplace, and B. Jolibois, *C. R. Acad. Sci. Paris* Ser. **C,** 1112 (1969).
16. J. Bernard, F. Theobald, and A. Vidonne, *Bull. Soc. Chim. Fr.*, (6), 2108 (1970); JCPDF card no. 23-790.
17. E. Andrukaitis, P. W. M. Jacobs, and J. W. Lorimer, *Can. J. Chem.* **68,** 1283 (1990).
18. M. E. Lines, *J. Phys. Chem. Solids* **31,** 101 (1970).
19. W. E. Hatfield, *J. Appl. Phys.* **52,** 1985 (1981).
20. B. Bleaney and K. D. Bowers, *Proc. R. Soc. London A* **214,** 451 (1952).